

# Application of an integrated CFD model to the metallic nanoparticle production in an Inductively coupled plasma reactor

*Silvânia Lopes\**, *Pierre Proulx\*\**, *Jean-Baptiste Gouriet\** and *Patrick Rambaud\**

*\*von Karman Institute for Fluid Dynamics*

*72 Chaussée de Waterloo, Rhode-Saint-Genèse, BELGIUM*

*\*\*Chemical Engineering department, University of Sherbrooke*

*2500 Boul. de l'Université, Sherbrooke, Quebec, CANADA*

## Abstract

A model has been developed to assist the design and operation of an inductively coupled plasma reactor process for the production of metallic nanoparticles. The model describes the plasma flow, the plasma-particles interaction and the nanoparticles formation by solving the Navier-Stokes, and the thermal energy equations coupled with the Maxwell equations formulated as vector potential equations; the lagrangian particle trajectory equations, including two-way coupling with the plasma flow; the nanoparticle Population Balance Equation (PBE) accounting for particle nucleation and growth, formulated using the method of moments; and the mass diffusion equation. The model is used to optimize the operating conditions of the reactor and to predict the production of nanoparticles. The results show the strong influence of the torch and quenching design on the final particle size distribution.

## 1. Introduction

Nanotechnologies, especially nanoparticles related applications, have recently received tremendous interest due to the great innovative potential they offer. The small size of the nanoparticles is responsible for many changes in the thermo-physical properties compared with the bulk materials, which makes them suitable for novel applications. Examples of these new properties include lower melting temperature, improved hardness and ductility, high self-diffusion coefficient, catalytic activity, and improved optical and electronic properties.

The processes used to generate the nanoparticles play an important role in terms of particles size, morphology, crystalline phase and composition, which fundamentally determine the properties of the nanostructure material. Thermal plasma processing, and in particular high-frequency inductively coupled plasma (ICP) reactor, consisting of a plasma torch which ensures the evaporation of injected micro precursor and a quenching reactor which ensures the synthesis of the nanoparticles by cooling of the vapor, have shown several distinctive advantages over other synthesis routes for nanoparticles [5] [10] [9]. Due mainly to its high temperature and energy density, as well as the large plasma volume and long residence/reaction time, it is considered relatively easy, in principle, to evaporate all injected precursor. Additionally, an ICP is generated without any internal electrodes and therefore the final product is free of contamination from electrodes aging and it offers the possibility to work under a controlled atmosphere. However neither the precise control of the particle size, distribution and morphology nor mass production has been successfully achieved in practice. The effects of the plasma torch and quenching parameters, including reactor design and configuration, on the flow field and on the formation of the nanoparticles appear to be of enormous importance [5].

Modeling studies can play an important role in the development and improvement of the nanoparticles synthesis processes, providing an insight into the phenomena involved and helping to identify the right operating conditions to employ. However, a full theoretical description of particles dynamics in plasma flows within an actual industrial environment is very complex. A complete model of such a system requires the solution of the fluid mechanics equations of continuity, momentum and energy, coupled with the electromagnetic field equations, which describe the generation of the plasma flow; with the description of micro particles evaporation in plasma flow; and with the nanoparticle population balance equation, describing the nanoparticles formation.

Nanoparticles are formed due to numerous coexisting mechanisms, such as nucleation, condensation, coagulation and surface reaction. Several methods have been developed to represent the evolution of a population of particles,



## 2. Model description

The overall integrated model developed to optimize the ICP reactor design consists of two parts which are solve simultaneously. The first part concerns the modeling and design of inductive argon plasma used for micro particles evaporation. It essentially presents the fluid dynamics of the plasma flow coupled with the electromagnetic field in the presence of particle precursor. The second part deals with the formation of nanoparticles accounting for nucleation and growth by condensation and coagulation of the metallic vapor transported with the plasma gas into the reactor zone, considering different mechanisms of transport.

### 2.1 Plasma-particle interaction model

For high powered plasma torch, the presence of the powder will have two effects. First the heat extracted by the powder from the plasma could cause substantial local cooling of the gas. Secondly, the evaporated fraction of the particles diffuses in the plasma gas and can drastically change its thermodynamic and transport properties, e.g. electrical conductivity and radiation losses.

#### 2.1.1 Governing equation for LTE

Modeling of electromagnetic fluid dynamic fields has been done aiming the description of the plasma temperature and flow fields in the induction zone, on the assumption of local thermodynamic equilibrium (LTE) condition. The thermodynamic and transport properties of the plasma are obtained in function of the operating pressure and flow temperature ( $p_0, T$ ) by means of formula based up on semi-classical statistical mechanical and kinetic theory [4]. The ICP torch modeling is done by extending the calculating domain of the electromagnetic field, imposed by the coil current, well outside of the plasma discharge region. The motion of the plasma is described using a system of Navier-Stokes equations and the solution of the electromagnetic field is derived from the simplified form of the Maxwell equations. The coupling between these two systems of equations is realized by the Lorentz force acting on the charged particles, Joule dissipation which heats up the plasma and through the dependence of electrical conductivity on temperature and operating pressure. The model is developed under the assumption of steady state, turbulent flow and the radiative heat transfer is based on the net emission coefficient approach. The continuity, momentum and energy equations in their general form can be expressed as follow:

$$\nabla \cdot (\rho \mathbf{u}) = S_p^c \quad (1)$$

$$\rho \mathbf{u} \cdot \nabla (\mathbf{u}) = -\nabla p + \nabla \cdot \mu_{eff} \nabla \mathbf{u} + F_{lz} + S_p^m \quad (2)$$

$$\rho \mathbf{u} \cdot \nabla (C_p T) - \nabla \cdot k_{eff} (T) = P_J + R + S_p^E \quad (3)$$

where  $\mathbf{u}$  is the flow velocity.  $\rho$ ,  $\mu$ ,  $k$ ,  $c_p$ , are the fluid density, dynamic viscosity, thermal conductivity, specific heat at constant pressure, respectively.  $T$  is the temperature,  $p$  is the pressure, and  $P_J$  and  $R$  are the Joule heating and the radiation loss, respectively.  $S_p^c$ ,  $S_p^m$  and  $S_p^E$  are the contributions of the particles to the transport of mass, momentum and enthalpy respectively. The Lorentz forces and the Joule heating are expressed as:

$$F_{lz} = -\frac{1}{2} \mu_0 \sigma \omega Re [\mathbf{A} \times \mathbf{H}] \quad (4)$$

$$P_J = \frac{1}{2} \sigma Re [E_\theta E_\theta^*] \quad (5)$$

The electromagnetic field induced in the plasma is expressed as the vector potential formulation of the Maxwell equations:

$$\nabla^2 \mathbf{A} = -\mu_0 (j_{coil} + j_{ind}) \quad (6)$$

where  $j_{coil}$  is the current density imposed in the coil and  $j_{ind}$  is the current induced in the plasma. For the standard induction plasma torch, if the coil is assumed to be composed of parallel rings, the vector has only an azimuthal component  $\mathbf{A} = (0, A_\theta, 0)$  [6]. The electromagnetic fields can be obtained by the following relation after solving the vector potential equation:

$$E_\theta = -i\omega A_\theta \quad (7)$$

$$\mathbf{H} = -\frac{1}{\mu_0} \nabla \times \mathbf{A} \quad (8)$$

where  $\mu_0$  is the magnetic permeability of free space,  $\sigma$  is the electrical conductivity. The superscript \* represent the conjugate and  $Re$  the real part of a complex number.

### 2.1.2 The particle precursors trajectory and heat transfer equations

Particle precursors are treated following the Lagrangian approach, which means that the parameters of every particle are in function of time. However, the mean characteristic of the particle in a sufficiently long period of time do not change, and we can consider them as stationary. Assuming that the only forces acting on an individual particle trajectory are the drag and gravity, the momentum equation for a single particle injected in the plasma can be expressed as:

$$m_p \frac{d\mathbf{u}_p}{dt} = C_D \frac{1}{2} \rho \left( \frac{1}{4} \Pi d_p^2 \right) (\mathbf{u} - \mathbf{u}_p) |\mathbf{u} - \mathbf{u}_p| + m_p g \quad (9)$$

It is assumed that the particles are spherical, and there is negligible internal resistance to heat transfer, i.e the particle is at uniform temperature throughout. The particle temperature is determined by an heat balance relating the convective heat transfer and the radiation losses at the particle surface:

$$Q = h_c A_p (T_\infty - T_p) - \epsilon A_p \sigma (\theta_R^4 - T_p^4) \quad (10)$$

where  $Q$  is the net heat exchange between the particles and its surroundings.

$$Q = \begin{cases} m_p C_p \frac{dT_p}{dt} & \text{if } T_p < T_{melt} \text{ and } T_{melt} < T_p < T_{Boil} \\ m_p H_m \frac{dx}{dt} & \text{if } T_p = T_{melt} \\ -\frac{\Pi}{2} \rho_p d_p^2 H_v \frac{dd_p}{dt} & \text{if } T_p > T_{boil} \end{cases} \quad (11)$$

The drag coefficient  $C_D$  and the heat transfer coefficient  $h_c$  are estimated using the following relations [11]:

$$C_D = \begin{cases} \frac{24}{Re_p} & \text{if } Re \leq 0.1 \\ \frac{24}{Re_p} \left( 1 + \frac{1}{6} Re_p^{2/3} \right) & \text{if } 0.1 \leq Re \leq 1000 \\ 0.44 & \text{if } Re_p > 0.1 \end{cases} \quad (12)$$

and

$$Nu = 2.0 + 0.6 Re^{1/2} Pr^{1/3} \quad (13)$$

where  $Re$  is the Reynolds number based on the particles diameter and the relative speed between the particles and the gas, and  $Pr$  is the Prandtl number. The source/sink terms in the corresponding gas phase continuity, momentum and energy equations are:

$$S_p^c = \sum \frac{N}{V} \Delta m_p \quad (14)$$

$$S_p^m = \sum \frac{N}{V} \Delta (m_p \mathbf{u}_p) \quad (15)$$

$$S_p^e = \sum \frac{N}{V} \int_0^\tau h_c A_p (T_\infty - T_p) \quad (16)$$

where the ration  $N/V$  is the concentration of particle  $N$  in a given cell volume  $V$  [7]. The thermodynamic and transport properties of the argon-vapor mixture are obtained using the database of VKI Mutation library[4] and radiation losses from the reference [8].

## 2.2 Nanoparticle Model

The formation and growth of nanoparticles by homogeneous nucleation, condensation and coagulation from a gas phase is the principal method of nanoparticles production. This process requires a supersaturated vapor, usually produced by the cooling of the vapor. This supersaturation state leads to the formation of the metallic nuclei by homogeneous nucleation, which will grow upon further increase on supersaturation. Since the number of particles formed is large, and since each particle can have a multitude of physical and chemical characteristics, a description that account for particles individually is not sought. Rather, one considerer a particle distribution function based on the particles properties and size. This particle distribution function ( $n_j$ ) represent the expected number of particle per  $m^3$  of size  $j$  in a control volume due to the particle growth and transport mechanism.

### 2.2.1 Particle nucleation.

Homogeneous nucleation is the formation of particles from a supersaturated vapor, which is caused by the fast cooling of the gas. The molecules (monomers) will form stable particles if the critical cluster size ( $d_p^*$ ) is less or equal to the molecule size of the vapor species surface [3]. The critical cluster size is:

$$d_p^* = \frac{4\sigma v_1}{k_B T \ln S} \quad (17)$$

where  $\sigma$  is the surface tension and  $S$  the saturation ratio (ratio of the monomer concentration  $n_s$ , to the monomer concentration at saturation  $n_{ss}$ ) and  $v_1$  is the volume of the molecule. The equation describing the evolution of the concentration  $n_j$  of the stable particles of size  $j$  by nucleation is:

$$\frac{dn_j}{dt} = I \delta_{j-j^*} \quad (18)$$

where  $\delta_{j-j^*}$  is defined as 1 for critical size  $j^*$  and zero otherwise. The nucleation rate ( $I$ ) is given by [2]:

$$I = \frac{\beta_{11} n_s^2 S}{12} \sqrt{\frac{\Theta}{2\pi}} \exp\left(\Theta - \frac{4\Theta^3}{27 \ln^2 S}\right) \quad (19)$$

where  $\beta_{11}$  is the Brownian collision coefficient between two monomer and  $\Theta$  the dimensionless surface energy.

### 2.2.2 Particle Growth-Condensation

The condensation phenomena is referred as the deposition of molecules from the gas phase on the stable particles surface [12]. It is described by the rate of volume change of the particle of size  $j$ , defined as:

$$G_j = \frac{dv_j}{dt} = B_1 v_1 j^{2/3} (S - 1) \quad (20)$$

In case of collision between a monomer of negligible size with particles of size  $j$  ( $d_j$ ), the collision coefficient in free molecular regime is given by:

$$\beta_1 = (36\pi)^{1/3} n_s v_1^{2/3} (k_B T / 2\pi m_1)^{1/2} \quad (21)$$

where  $n_1$  and  $m_1$  are the concentration and mass of the vapor molecule, respectively.

### 2.2.3 Particle Coagulation

Coagulation is the interparticle phenomenon wherein nanoparticles collide with one another, due to a relative motion between them and adhere to form a larger particle. After the instantaneous nucleation, the particles coalesce due to the brownian movement. This phenomena is described by the Smoluchowski master equation, which expresses the time evolution of the particle population by an infinite set of differential equation:

$$\frac{dn_j}{dt} = \frac{1}{2} \sum_{i=j^*}^{j-1} \beta_{i,j-1} n_i n_{j-1} - n_j \sum_{i=j^*}^{\infty} \beta_{i,j} n_i \quad (22)$$

Because most of the particles are smaller than the mean free path of the gas, the Brownian motion is assumed in free molecular regime. In this case, the collision frequency between particles of size  $j$  and  $i$  is expressed as following [1]:

$$\beta_{i,j} = 2.2 \sqrt{\frac{6k_B T}{4\rho}} \left(\frac{3m_1}{4\pi\rho}\right)^{1/6} \sqrt{\frac{1}{m_i} + \frac{1}{m_j}} \left(m_i^{1/3} + m_j^{1/3}\right)^2 \quad (23)$$

### 2.2.4 Brownian Diffusion

In case of small particles flowing in the high temperature zones of the reactor, the Brownian motion becomes important. The diffusion coefficient of particle of size  $d_j$  is then the sum of the laminar and the turbulent components:

$$\mathfrak{D}_j = \frac{k_B T}{3\pi\mu d_j} \left(1 + \frac{3.31\lambda}{d_j}\right) + \nu^t \quad (24)$$

The evolution of the concentration  $n_j$  of stable particle of size  $j$  due to Brownian diffusion is given by:

$$\frac{dn_j}{dt} = \vec{\nabla} \cdot (\mathfrak{D}_j \nabla n_j) \quad (25)$$

### 2.2.5 Thermophoresis

Thermal deposition of particles occurs when a temperature gradient is present in a flow with the small particles experiencing a force in the direction of decreasing temperature. For small particles, the thermal force is a result of a greater transfer of momentum from the gas molecules of the hot zone relative to the cold zone. In this case, the thermophoresis velocity is independent of the particle size and directly proportional to the gradient of temperature, given by Waldmann and schmitt (1966) as:

$$\vec{u}_{th} = -\frac{0.55\mu}{\rho T}\vec{\nabla}T \quad (26)$$

For simplicity, the deposition of the particles at the walls is considered by fixing the total concentration of particle at the wall boundary equal to zero, which means that all the particles touching the wall will deposit on it and will not be accounted in the fluid volume anymore.

### 2.2.6 Method of Moment

To describe the formation of nanoparticles, the particle size distribution are obtained by solving the general dynamic equation for aerosol growth, which describes the evolution of the particle size distribution function  $n(v, t)$ , taking into account the contribution of the growing and transport mechanisms [12]:

$$\vec{\nabla} \cdot (\vec{u}n_j) = \underbrace{-\vec{\nabla} \cdot (\vec{u}_{th}n_j)}_{\text{thermophoresis}} + \underbrace{\vec{\nabla} \cdot (\mathfrak{D}_j \nabla n_j)}_{\text{diffusion}} + \underbrace{I\delta_{j-j^*}}_{\text{nucleation}} + \underbrace{G_{j-1}n_{j-1} - G_j n_j}_{\text{condensation}} + \underbrace{\frac{1}{2} \sum_{i=j^*}^{j-1} \beta_{i,j-1} n_i n_{j-1} - n_j \sum_{i=j^*}^{\infty} \beta_{i,j} n_i}_{\text{coagulation}} \quad (27)$$

However, it is generally difficult to solve Eq. 27 because of its nonlinearity. A physically realistic dependence of the collision coefficient  $\beta_{ij}$  on the sizes of the colliding particles makes it impossible to obtain a closed-form solution. The method of moment reformulates the problem into a small set of equations with the  $k^{\text{th}}$  moment  $M_k$  defined as:

$$M_k = \frac{1}{\rho n_0} \sum_{j=j^*}^{\infty} j^k n_j \quad (k = 0, 1, 2, \dots) \quad (28)$$

The moments of the size distribution are normalized with respect to the density  $\rho$  and the initial monomers concentration  $n_0$  at the entrance of the reactor. The collision coefficients is then evaluated in terms of the reduced moments  $\mu_r = M_r/M_0$  of fractional order, and calculated from a Lagrangian interpolation between the logarithms of the related function  $f_{0,0}^r$ , and defined as  $\phi_{0,0}$ :

$$\phi_{0,0} = C (f_{0,0}^0)^{3/8} (f_{0,0}^1)^{3/4} (f_{0,0}^2)^{-1/8} \quad (29)$$

where the coefficient  $C$  is

$$C = \sqrt{\frac{8\pi k_B T}{m_1}} \left( \frac{2m_1}{4\pi\rho_p} \right)^{2/3}. \quad (30)$$

The functions  $f_{0,0}^r$  are obtained from the reduced moments of fractional order:

$$f_{0,0}^0 = 2(\mu_{-1/2}\mu_{1/6} + \mu_{-1/6}^2) \quad (31)$$

$$f_{0,0}^1 = 2(\mu_{-1/2}\mu_{7/6} + 2\mu_{-1/6}\mu_{5/6} + \mu_{1/6}\mu_{1/2}) \quad (32)$$

$$f_{0,0}^2 = 2(\mu_{-1/2}\mu_{13/6} + 2\mu_{-1/6}\mu_{11/6} + \mu_{1/6}\mu_{3/2} + 2\mu_{1/2}\mu_{7/6} + 2\mu_{5/6}^2) \quad (33)$$

This method, so-called MOMIC was proposed and validated by Frenlach and Harris [1]. In MOMIC, the fractional moments order are determined by interpolation among whole moments whose values are available at each iteration step. The definition of the moments of size distribution leads to the reformulation of the conservation equations (Eq. 27) describing the evolution of the moments of the particle size distribution functions (PSDF), in terms of moments as:

$$\frac{\partial(\rho M_k)}{\partial t} + \vec{\nabla} \cdot (\rho \vec{u} M_k) = \underbrace{-\vec{\nabla} \cdot (\rho \vec{u}_{th} M_k)}_{\text{thermophoresis}} + \underbrace{\vec{\nabla} \cdot (\rho \mathfrak{D} \vec{\nabla} M_k)}_{\text{diffusion}} + \underbrace{\frac{I}{n_0} (j^*)^k}_{\text{nucleation}} + \underbrace{k\beta_{1\rho} (S-1) M_{k-1/3}}_{\text{condensation}} + \underbrace{\frac{\rho^2 n_0}{4} [k^2 + k - 2] \Phi_{0,0} M_{k/2}^2}_{\text{coagulation}} \quad (34)$$

Using the hypothesis of log-normal particle size distribution, it is possible to calculate the different moments of the particle size distribution in a close form using only the few moments of distribution. The principal physical properties of the PSDF (mass mean diameter, standard deviation) are obtained from the moments distributions, as defined on table

Table 2: Principal physical properties of PSDFs

|  |  |
|--|--|
| Total concentration                    | $M_0$  |
| Mean numerical diameter                | $d_1 M_{1/3} / M_0$  |
| Mean mass diameter                     | $d_1 M_{4/3} / M_0$  |
| Width of mean mass diameter $\sigma^2$ | $d_1^2 \left( \frac{M_{5/3}}{M_0} - \frac{M_{4/3}^2}{M_0^2} \right)$ |
| Mean surface                           | $s_1 M_{2/3} / M_0$  |
| Mean volume                            | $v_1 M_1 / M_0$  |

2 [3]. Therefore, a closed system of the equation can be obtained to describe the evolution of the moments distribution in function of its own properties. In this study, only the first three moments of the particle size distribution function are used. The moments  $M$  of order 0 and 1 are the number concentration and mass of the particles in a given volume, respectively. The moment of order 2 is also known to be proportional to the light scattered by the nanoparticles when they have much smaller size than the wavelength of the incident light. These conservation equations can be solved with the flow equation to describe the spatial distribution of the moments in the flow field. The conservation of monomer in vapor phase is obtained by the mass balance over the nanoparticles and the vapor, as follow:

$$\frac{\partial(\rho\omega_1)}{\partial t} + \vec{\nabla} \cdot (\rho\vec{u}\omega_1) = \vec{\nabla} \cdot (\rho\mathfrak{D}_1\vec{\nabla}\omega_1) - Ij^*m_1 + \beta_1\rho n_0 m_1 (S - 1) M_{k-1/3} + S_p^c \quad (35)$$

### 3. Model implementation

The implementation of the full coupled plasma inductively model, lagrangian particle evaporation model, and nanoparticles formation model is done using the OpenFoam source code. In OpenFOAM the flow equations are described by a system of linked partial differential equations and the code itself is a collection of object-oriented routines developed for the manipulation of tensor fields. Coupling between equations is treated using a segregated approach, in which equations are formulated for each dependent variable and solve sequentially, with the possibility of iteration over the system of equations until convergence is achieved. OpenFOAM has been designed from the start for 3-dimensional space and defines all geometrical grids or meshes as such. However, two dimensional and axisymmetric problems can be simulated by generating a mesh in 3 dimensions and applying special boundary conditions on any patch in the plane normal to direction of interest. More especially for axisymmetric problems, the geometry is specified as a wedge of 5 degrees angle and one cell thick running along the plane of symmetry. In this study the geometry is also considered as 2D axisymmetric, specified as a wedge of a 5 degrees angle composed of 135000 cells (see figure 1). The quenching system consists of two quenching units, positioned perpendicularly to the plasma jet axis. The quenching inlet is therefore a uniform slot (which corresponds to an annular injection around the quench unit). Computations are carried out for the inductively coupled plasma torch operated with argon at atmospheric pressure, with a dissipated power of 5kW and a mass flow of argon of 0.6g/s. Precursor particles of 30  $\mu m$  is injected into the torch at a rate of 0.3 and 0.6  $g/min$ . The position of the first and second quench units and its respective intensity and injection angle are here also studied in order to determine the better conditions for fast cooling without a large perturbation of the flow. Detailed description of the operating conditions are presented in table 1.

## 4. Results and Discussion

### 4.1 Effects of particle loading on the temperature field

A detailed study of the micro particle precursor injection is made taking into account the 2-way coupling with the plasma flow and the changes on the plasma gas properties, namely electrical conductivity and radiation losses, due to the presence of metallic vapor. Figure 2 shows the temperature field and the concentration of the metal vapor in the torch for the case of no particle, 0.3 and 0.6  $g/min$  precursor feed-rate. It is shown that even for very low particle loading ratios, i.e. 0.3  $g/min$ , the local decrease of the temperature field in the plasma is still unexpectedly pronounced. While the relative mass loading is well below 1%, a decrease of more than 2000  $K$  is still observed along the centerline of the plasma as can be seen in figure 3. These results show that even for condition which are generally assumed to be safe to neglect the change in plasma temperature due to particle injection, the cooling effect can be significant. The importance of the direct coupling plays a role, but most of the two-phase coupling is in this case due to the important changes in plasma properties and plasma radiation. In the case of 0.3  $g/min$  particles are mostly evaporated in the torch

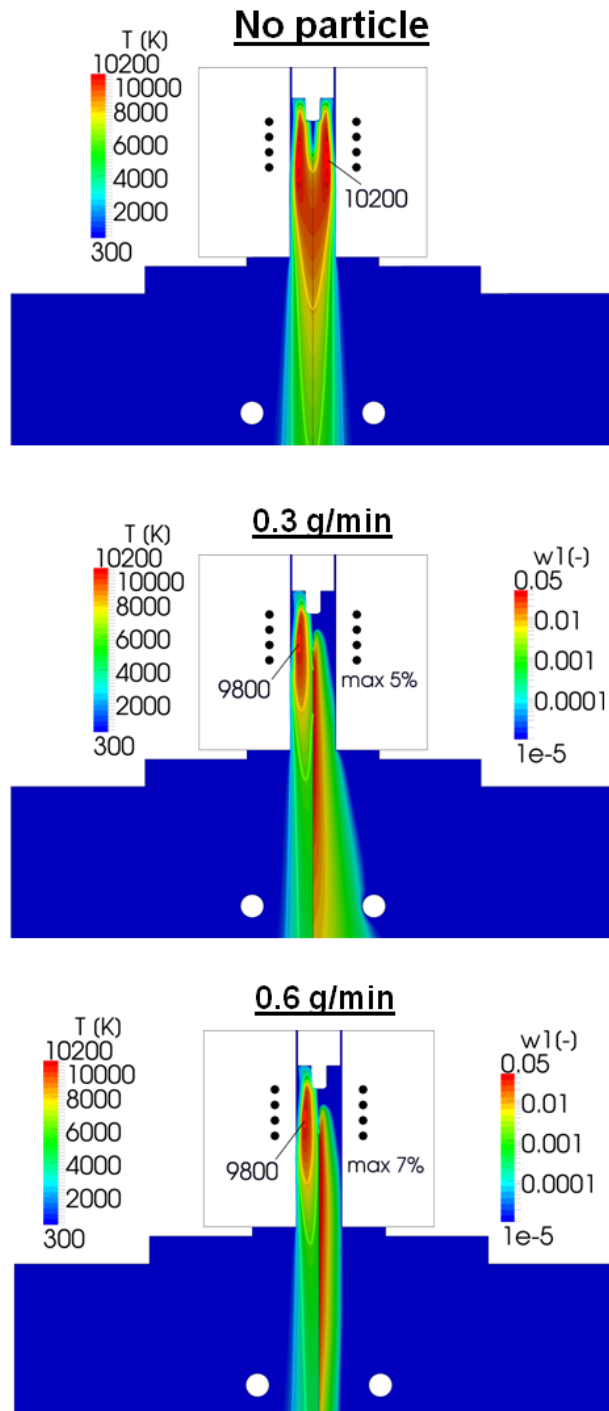


Figure 2: Temperature and vapor concentration for different precursor feed-rate

zone and the vapor is afterward transported into the reactor, but for the case of  $0.6 \text{ g/min}$  particles are still evaporating in the reactor zone and this can be also observed by the patterns of the vapor concentration presented in figure 2.

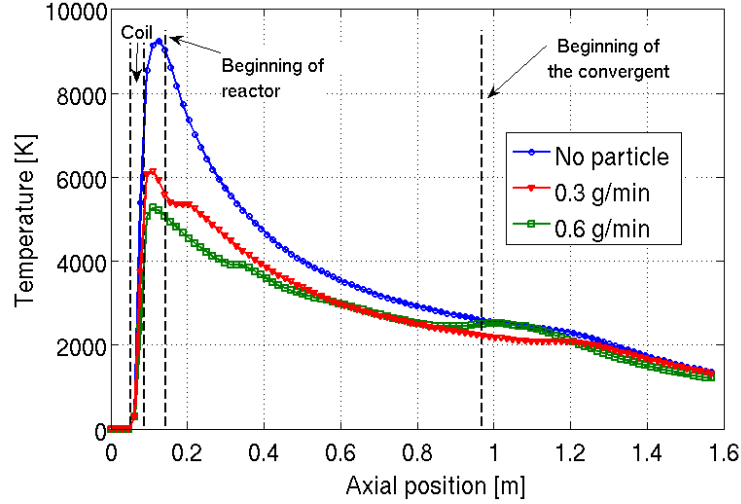


Figure 3: Effect of particle loading on the temperature field at the center line

#### 4.2 Effects of the quench on the nanoparticles formation

Table 3: Condition of the studied cases

|        | 1 <sup>st</sup> Quench |               | 2 <sup>nd</sup> Quench |               |
|--------|------------------------|---------------|------------------------|---------------|
|        | $Q_{q1}$ [slpm]        | $L_{q1}$ [mm] | $Q_{q2}$ [slpm]        | $L_{q2}$ [mm] |
| Case A | –                      | –             | –                      | –             |
| Case B | 35 (45°)               | 95            | –                      | –             |
| Case C | 35 (45°)               | 95            | 40 (60°)               | 195           |
| Case D | 35 (45°)               | 95            | 45 (60°)               | 195           |
| Case E | 35 (45°)               | 95            | 50 (75°)               | 195           |
| Case F | 35 (45°)               | 95            | 50 (80°)               | 195           |
| Case G | 35 (45°)               | 95            | 60 (75°)               | 195           |

The critical importance of the flow, temperature, vapor concentration patterns on the nucleation and growth of the nanoparticles is analyzed for different quench injection flow rate and angle, presented in table 3. An amount of  $0.6 \text{ g/min}$  of particle precursor is injected and evaporated in the plasma flow. Figure 4 presents the temperature field and vapor concentration for the case without quench, with 1 quench unit (Case A) active and with two quench units (Case G) active. As it can be seen, the quench units determine not only the cooling rate of the plasma jet in the reactor but also the patterns of the vapor diffused. The combination of these two fields will determine where the particles are created. The nucleation temperature of the vapor used (the temperature in which nucleation occurs) under these conditions is below 2000K. These means that the vapor needs to be cooled below this temperature for nucleation to occur. For the case without quench, the vapor is spontaneously transported to the end of the reactor but the temperature still very high, therefore only few amount of particles will be generated close to the cooled walls because of the weak presence of vapor in these region. Using one quench unit one can notice already a small cooling in the convergent part of the reactor but due to the configuration of the quench and the reactor the vapor tend to diffused and get caught in the recirculation zone which is developed in the reactor. This can cause growth of big and uncontrolled particles size. For the second quench, different configurations for injection flow rate and injection angle (Cases C-G) were tested in order to obtain a desired cooling of the plasma jet and a control on the diffusion of the vapor. The improvement is achieved when increasing the injection rate and angle as can it be seen also in figure 4 for the *case G*. It is shown that with this pronounced injection angle and rate, the cooling rate is prominent and the vapor is enforced into the center of the reactor.

The result of the implementation of the nanoparticle formation model is presented in figure 5, where one can see the concentration of the produced nanoparticles and the respective mass mean particle size. As referred before,

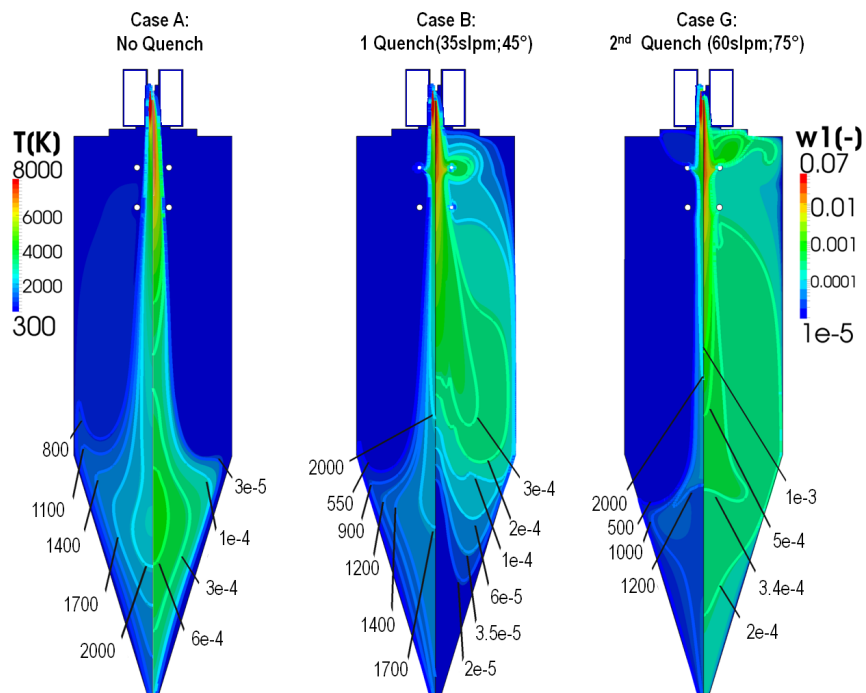


Figure 4: Temperature field(left) and vapor concentration (right)

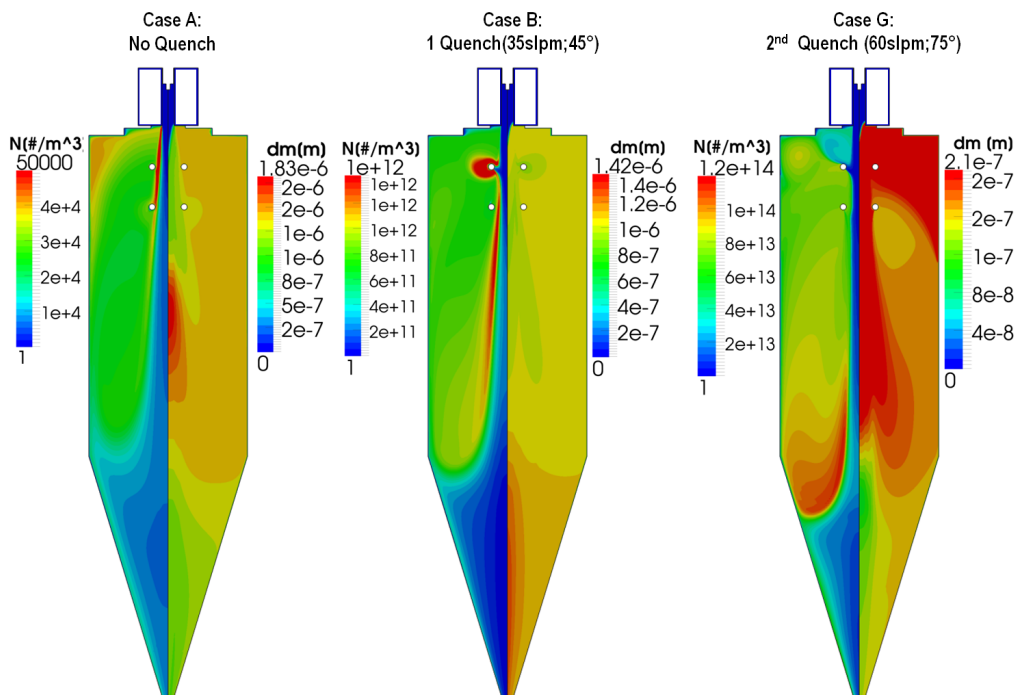


Figure 5: Concentration of nanoparticles (left) and mean mass diameter (right)

the generation of the nanoparticles is strongly dependent on the temperature and vapor field. For the case without, it is shown that only a very few amount of particles are in fact generated. For the case of using one quench unit, the results demonstrate that the particles are created in the recirculation zone reaching the size of  $1.4\mu\text{m}$  and leading to a high deposition of nanoparticles at the walls of the reactor. By activating the second quench, higher amount of particles are produced with smaller size diameter. The particle size distribution function at the exit of the reactor is presented in figure 6, for different quench configuration. It can be seen that using only one quench unit or both with the second quench at low injection flow rate and injection angle, the particles have a wider size distribution with an average diameter (mixing cup diameter  $D_{cup} = \int d_m \rho v \cdot d\vec{A} / \int \rho v \cdot d\vec{A}$ ) of around 1000nm. By increasing the cooling rate and the injection angle, it is possible to obtain particles with a narrow size distribution and mean diameter around 160nm. Table 4 summarizes the average mean mass diameter and the mass efficiency at the out of the reactor for the different quench configurations system.

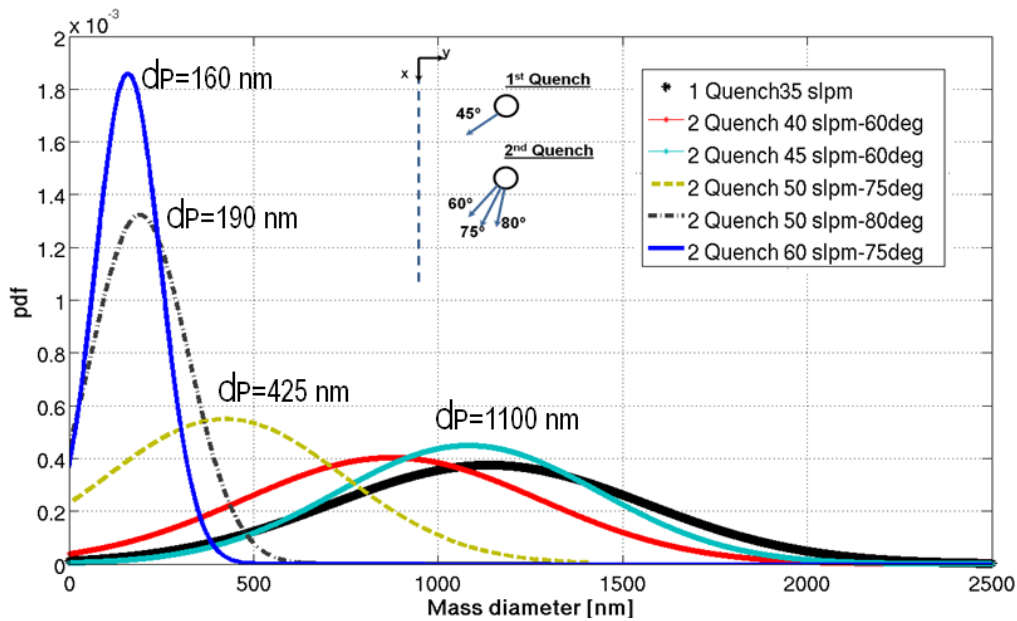


Figure 6: Particle size distribution at the outlet of the reactor (Effects of quench with respect to the cooling rate, angle and position)

Table 4: Summary of the mean mass diameter and mass efficiency at the outlet of the reactor

|        | $Q_{q1}$ [slpm] | $Q_{q2}$ [slpm] | $dp$ [nm] | $\epsilon$ [%] |
|--------|-----------------|-----------------|-----------|----------------|
| Case A | –               | –               | –         | –              |
| Case B | 35 (45°)        | –               | 1140      | 6              |
| Case C | 35 (45°)        | 40 (60°)        | 871       | 22             |
| Case D | 35 (45°)        | 45 (60°)        | 1000      | 10             |
| Case E | 35 (45°)        | 50 (75°)        | 425       | 38             |
| Case F | 35 (45°)        | 50 (80°)        | 190       | 48             |
| Case G | 35 (45°)        | 60 (75°)        | 160       | 8              |

## 5. Conclusions

A Multi-physical integrated model for prediction of nanoparticles formation in ICP reactor, describing the plasma flow, the plasma-particles interaction, the nucleation and growth of the nanoparticles using the method of moments is simultaneously implemented. The model has been developed to assist the design and operation of an inductively coupled plasma reactor process for the production of metallic nanoparticles. The effects of the micro particle precursor loading and the quench design on the temperature field and vapor field are investigated. The results show that even for low particle mass loading (less than 1%) the effects of the particle evaporation on the temperature field could be very significant, with a decrease of more than 2000K at the reactor center line. It also emphasizes that neglecting the

plasma-particle interactions at the present conditions could be unrealistic. The evaporation of the powders influences also the profile of the vapor concentration which enters in the reactor. It is also shown the influence of the quench design on the final particle size distribution. The quench strongly affects the temperature and the vapor concentration in the reactor and consequently has a decisive impact on the final particle size distribution, because of the strong coupling between the flow, temperature, and concentration field on the formation of nanoparticles. The first quench alone proved to be not very effective, creating particles on the range of  $1\mu\text{m}$  with high deposition at the walls. Activating the second quench unit at both low injection flow rate and injection angle does not provide significant improvement. On the contrary, increasing the quenching flow rate and the injection angle, provide a much smaller mass mean particle diameter ( $\approx 160\text{nm}$ ) and a narrower size distribution. At the outlet of the quenching reactor, the total mass of nanoparticles condensed is a measure of the mass conversion efficiency of the process. There are mostly two ways to improve this efficiency. The first one is to maximize the vapor condensation inside of the reactor in order to avoid it downstream of the reactor, in the piping system. The second one is to minimize the particle deposition at the walls of the reactor. In the future, different quench injection systems will be tested in order to optimize the mass conversion efficiency. This parametric study will also allow to determine the relevant process parameters to produce nanopowders of a desired granulometry.

### Acknowledgment

The financial support of this work is provided by the Walloon Region under the convention 6405 which is gratefully acknowledged.

### References

- [1] M. Frenklach. Method of moments with interpolative closure. *Chemical Engineering science*, 57:2229–2239, 2002.
- [2] S. L. Girshick and C. P. Chiu. Kinetic nucleation theory: A new expression for the rate of nucleation from an ideal supersaturated vapor. *J. Chem. Phys.*, 93:1273–1277, 1990.
- [3] William C. Hinds. *Aerosol Technology*. Wiley, 1999.
- [4] Thierry E. Magin. *A model for Inductive Plasma Wind tunnels*. PhD thesis, Université Libre de Bruxelles, 2004.
- [5] N. Mendoza-Gonzalez, Mbark El Morsli, and Pierre Proulx. Production of nanoparticles in thermal plasmas: A model including evaporation, nucleation, condensation and fractal aggregation. *Journal of Thermal Spray Technology*, 17(4):533–550, 2008.
- [6] S. Pai. *Magneto-gasdynamics and Plasma dynamics*. Springer-Verlag, 1962.
- [7] Mostaghimi J. Boulos M. Proulx, P. Plasma-particle interaction effects in induction plasma modelling under dense loading conditions. *Journal of Heat and Mass Transfer*, 28:1327–1337, 1985.
- [8] Mostaghimi J. Boulos M. Proulx, P. Radiation energy transfer in induction plasma modelling. *Journal of Heat and Mass Transfer*, 34:2571–2579, 1991.
- [9] C. Schreuders. *Synthèse par plasma inductif de nanométriques de silicium optimization de la trempe*. PhD thesis, Université de Limoges (France), 2006.
- [10] M. Shigeta and T. Watanabe. Numerical investigation of cooling effect on platinum nanoparticles formation in inductive coupled thermal plasma. *Journal of Applied Physics*, 103 (074903):1–15, 2008.
- [11] V. V. Wang G.-X. Sampath G. X. W. S. S. Fincke J. R. Wan Y. P., Prasad. Model and powder particle heating, melting, resolidification, and evaporation in plasma spraying processes. *Journal of Heat transfer-ASME*, 121:691–699, 1999.
- [12] Sudarshan K. Loyalka Williams M. M. R. *Aerosol Science: Theory and Practice: with special applications to nuclear industry*. Pergamon Press, 1991.